J Solid State Electrochem (2012) 16:1743–1751
DOI 10.1007/s10008-011-1598-y

ORIGINAL PAPER

Enabling the Li-ion conductivity of Li-metal fluorosulphates by ionic liquid grafting

Prabeer Barpanda · Rémi Dedryvère · Michael Deschamps · Charles Delacourt · Marine Reynaud · Atsuo Yamada · Jean-Marie Tarascon

Received: 1 August 2011 / Revised: 7 November 2011 / Accepted: 10 November 2011 / Published online: 30 November 2011

Abstract Recently unveiled 'alkali metal fluorosulphate ($AMSO_4F$)' class of compounds offers promising electrochemical and transport properties. Registering conductivity value as high as 10^{-7} S cm^{-1} in $NaMSO_4F$ phases, we explored the fluorosulphate group to design novel compounds with high Li-ion conductivity suitable for solid electrolyte applications. In the process, we produced sillimanite-structured $LiZnSO_4F$ by low temperature synthesis ($T \leq 300$ °C). Examining this phase, we accidentally discovered the possibility of improving the ionic conductivity of poor conductors by forming a monolayer of ionic liquid at their particle surface. This phenomenon was studied by solid-state NMR, XPS and AC impedance spectroscopy techniques. Further, similar trends were noticed in other fluorosulphate materials like tavorite $LiCoSO_4F$ and triplite $LiMnSO_4F$. With this study, we propose 'ionic liquid grafting' as an interfacial route to enable good Li-ion conductivity in otherwise poor conducting ceramics.

Keywords Conductivity · Fluorosulphates · Ionic liquid grafting · Solid electrolyte

P. Barpanda · C. Delacourt · M. Reynaud · J.-M. Tarascon
Laboratoire de Réactivité et Chimie des Solides,
CNRS UMR 6007, Université de Picardie Jules Verne,
33, Rue Saint Leu,
Amiens Cedex 80039, France

P. Barpanda (✉) · A. Yamada
Department of Chemical System Engineering,
The University of Tokyo,
Building 5-607, 7-3-1 Hongo, Bunkyo-ku,
Tokyo 113-8656, Japan
e-mail: prabeer@chemsys.t.u-tokyo.ac.jp

R. Dedryvère
IPREM-ECP, University of Pau,
Hélioparc Pau Pyrénées, 2 av. Pierre Angot,
64000 Pau, France

M. Deschamps
Cenre de Recherches sur les Materiaux a Hautes Temperatures,
CNRS UPR 3079,
1D Avenue de la Recherche Scientifique,
Orléans Cedex 45071, France

J.-M. Tarascon
Collège de France,
11 Place Marcelin Berthelot,
Paris 745005, France

Introduction

'Mobile energy supply' is increasingly becoming an integral part of modern life heavily relying on portable electronics, communication devices and automotive vehicles. Li-ion batteries, with their high gravimetric and volumetric energy density, are front runners in this sector. Lithium-ion battery technology got kick started with oxide-based ceramics (e.g., $LiCoO_2$) in the early 90s [1]. Later in 1997, olivine $LiFePO_4$ was introduced as a possible cathode material [2], which opened up the whole new world of 'polyanionic compounds', paving the way for the discovery of novel cathode materials such as Li_2MSiO_4, $LiMBO_3$, $LiMPO_4F$, $Li_2MP_2O_7$, etc. [3–6]. Exploring the polyanion chemistry, our group discovered a new cathode material, $LiFeSO_4F$, operating at 3.6 V (vs. Li/Li^+) with a reversible capacity in excess of 130 mAh g^{-1} [7]. It unraveled 'alkali metal fluorosulphates ($AMSO_4F$)' as a new family of compounds with potential electrochemical applications. Subsequent works on Li-based and Na-based fluorosulphate phases were realized within a year [8, 9]. Particularly, $NaMSO_4F$ phases having tavorite structure

(space group $P2_1/c$) showed high pressed pellet (green density ~77%) room temperature conductivity of ~10^{-7} S cm^{-1}. A higher value of intrinsic conductivity can be obtained with the realization of fully dense pellets. Although this conductivity value is lower than current generation solid-state electrolytes [10], it encouraged us to design other $AMSO_4F$ compounds with higher order conductivity suitable for solid electrolyte application in all-solid-state battery technology.

This sets our goal to make a fluorosulphate-based solid-electrolyte material. It should address three major criteria: (i) excellent ionic conductivity, (ii) wide electrochemical stability window, and (iii) feasibility of low temperature synthesis as $AMSO_4F$ compounds are prone to decomposition at high temperature. We zeroed in to synthesize $LiZnSO_4F$ as its precursor $ZnSO_4{\cdot}H_2O$ is isostructural to other $MSO_4{\cdot}H_2O$ precursors and Zn is electrochemically inactive (hence, stable). Using a two-step low temperature synthesis method (ionic liquid or solid-state synthesis) [8], we successfully produced sillimanite-structured $LiZnSO_4F$. Performing conductivity measurement, we accidentally discovered that the involvement of ionic liquids during synthesis led to six orders of improvement in effective ionic conductivity of $LiZnSO_4F$ [11]. Combining several techniques such as solid-state Nuclear Magnetic Resonance (SS-NMR), X-ray Photoelectron Spectroscopy (XPS) and AC impedance spectroscopy, here we report a detailed spectroscopy analysis of ionic liquid-prepared $LiZnSO_4F$ samples. The presence of a thin layer of ionic liquid attached to particles' surface (i.e., ionic liquid grafting) led to the formation of ceramic–ionic liquid composites. The surface ionic liquid graft, being slightly Li^+-rich, was found to be responsible for the conductivity improvement. Similar trends were also observed in some other isostructural $LiMSO_4F$ phases. The transport properties of ceramic materials can be improved by forming a conducting coating at their interface (e.g., carbon coating [12]). The current paper presents 'ionic liquid grafting' as a surface modification to enable the Li-ion conductivity of inherently poor conducting ceramics, which can be applied in realizing next generation solid electrolytes.

Experimental

Synthesis of alkali metal fluorosulphates

The $ZnSO_4{\cdot}H_2O$ monohydrate precursor was prepared from commercially procured $ZnSO_4{\cdot}7H_2O$ by removing six-units of extra structural water by annealing it at 150 °C for 1 h either by (i) primary vacuum, i.e., ceramic route ($ZnSO_4{\cdot}H_2O$-C) or (ii) immersing inside EMI-TFSI ionic liquid, i.e., IL route ($ZnSO_4{\cdot}H_2O$-IL). Following, $LiZnSO_4F$ was prepared by (i) mixing LiF and $ZnSO_4{\cdot}H_2O$ in 1:1 molar ratio, (ii) pressing the precursor powder (at 10 bars) to form pellets, (iii) loading the pellets inside a Teflon-lined Bomb Parr reactor, and (iv) heating the Parr reactor at 300 °C for 30–40 h (heating rate=2 °C/min) before cooling down to room temperature. Depending on the precursor, the final products were abbreviated as $LiZnSO_4F$-C or $LiZnSO_4F$-IL. Following this procedure, $LiCoSO_4F$ and $LiMnSO_4F$ was prepared at 300 °C by using $CoSO_4{\cdot}H_2O$ and $MnSO_4{\cdot}H_2O$ precursors respectively. X-ray powder patterns were collected with a Bruker D8-Advantage powder diffractometer using Cu-Kα source (λ_1=1.5403 Å) (operating at 40 mA, 40 kV) and a LynxEye detector. Crystal structures were solved by Rietveld refinement using the FullProf program [13] and the structures were drawn using the Vesta software [14]. SEM images were obtained via an FEI Quanta 200-F SEM unit in low vacuum mode (operating voltage 20 kV).

Spectroscopy characterizations of fluorosulphate samples

AC impedance spectroscopy was conducted using a Bio-logic VMP3 unit. The fluorosulphate samples were pressed combining uniaxial (~10 bars) and isostatic (~2,500 bars) press to form dense pellets (~77% theoretical density). Ionically blocking electrodes were prepared by gold sputtering on both faces of the pellets. Ionic conductivity was measured over the temperature range of RT–140 °C by employing ac impedance spectroscopy (signal: 200 kHz–10 mHz). Li-ion mobility in these samples was further tested by applying a fixed voltage (25–100 mV) and recording the DC current in the pellets sandwiched between two sheets of PEO (saturated in 1 M $LiClO_4$) and Li-foils.

The room-temperature solid-state NMR study was performed by using a 7-T Bruker Avance NMR spectrometer operating at 300 MHz for ^{1}H, 117 MHz for ^{7}Li and 282 MHz for ^{19}F, respectively. We used a 1.3-mm double resonance probe for ^{1}H and ^{19}F (operating at a 60-kHz MAS rate) and a 4-mm double resonance probe for ^{7}Li (operating at a 14-kHz MAS rate). Recycling delay value was set to 120 s (for ^{1}H and ^{19}F) and 1 s (^{7}Li), respectively. For ^{1}H and ^{19}F, the RF fields for the 90° excitation pulses were set to 150 and 200 kHz, respectively and four transients have been recorded. Sixteen transients were recorded for ^{7}Li with a 1.1-μs long $\pi/12$ excitation pulse. The chemical shifts were referenced with 4-acetophenone at δ=−107 ppm for ^{19}F, TMS at 0 ppm for ^{1}H and 1 M LiCl at 0 ppm for ^{7}Li. The variable temperature NMR spectra were realized on a 9.4-T Bruker Avance NMR spectrometer operating at 400 MHz for ^{1}H, 155 MHz for ^{7}Li and 376 MHz for ^{19}F, respectively, using a 4-mm Bruker WVT probe with liquid nitrogen cooling and using a 5-kHz and 10-kHz MAS rate at low temperatures and high temper-

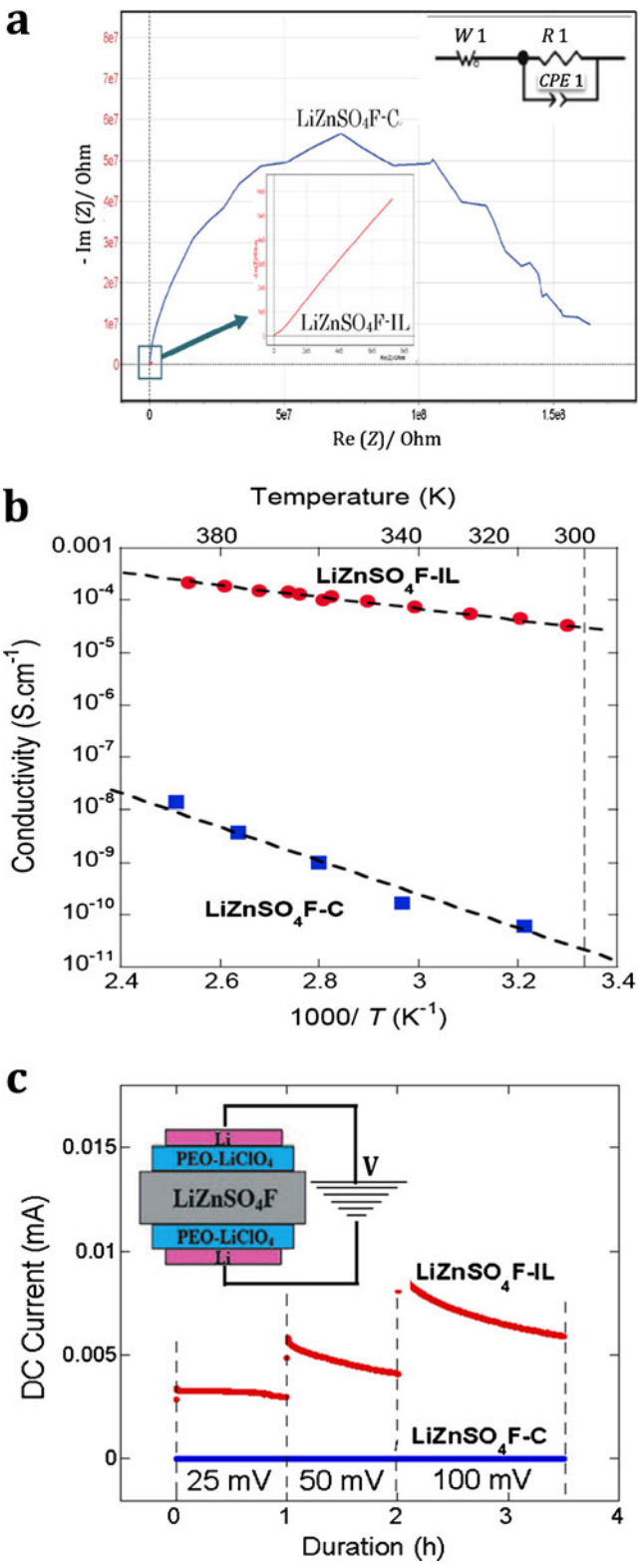

Fig. 1 Transport properties of $LiZnSO_4F$-C and $LiZnSO_4F$-IL samples. **a** Comparative Nyquist plots showing a large semicircle for $LiZnSO_4F$-C and a large Warburg diffusion line for $LiZnSO_4F$-IL materials. The *inset* presents the equivalent circuit diagram comprising of a resistance (*R*1) and a constant phase element (*CPE*1) in parallel connection with a Warburg resistance (*W*1). **b** Arrhenius plots of ac conductivity showing six-order increment in the conductivity in the case of $LiZnSO_4F$-IL ($\sim 10^{-5}$ S cm^{-1}) in comparison to $LiZnSO_4F$-C ($\sim 10^{-11}$ S cm^{-1}). **c** Polarization DC current measurement (at different voltages) of $LiZnSO_4F$-IL and $LiZnSO_4F$-C pellets sandwiched between PEO:$LiClO_4$ sheets and Li foils. The detail Swagelok architecture is shown in the *inset*

atures, respectively. Sixteen transients were recorded for ^{7}Li with a 3.9-μs long $\pi/12$ excitation pulse. The RF excitation field for ^{19}F was set at 93 kHz, and in both cases, the recovery delay was 10 s. The temperature was calibrated using the ^{207}Pb chemical shift of $PbNO_3$ [15].

XPS analysis was carried out using a Kratos Axis Ultra spectrometer using focused monochromatized Al Kα radiation ($h\nu$=1,486.6 eV). The spectrometer was calibrated using the photoemission line Ag 3 $d_{5/2}$ (binding energy= 368.3 eV) and the pressure in the analysis chamber was maintained at 5×10^{-7} Pa. The analyzed area of the samples was 300×700 μm^2. Core peaks were recorded with a 20-eV constant pass energy. Due care was taken to avoid moisture/air exposure to test specimens. The XPS spectrometer was directly connected through a transfer chamber to an argon dry box. Core peaks were analyzed using a nonlinear Shirley-type background and peak positions and areas were obtained by weighted least-square fitting of model curves (70% Gaussian+30% Lorentzian) to the experimental data.

Results and discussion

To gauge the feasibility of using low-temperature-synthesized $LiZnSO_4F$ as solid electrolyte, its ionic conductivity was analyzed by AC impedance spectroscopy. As shown in Fig. 1a, typical impedance spectrum of $LiZnSO_4F$-IL was dominated by a large Warburg diffusion line at nearly 45°, characteristic of ionic conductors. On the other hand, the impedance spectra of $LiZnSO_4F$-C sample consisted of a very large semi-circle with a negligible Warburg diffusion tail, hinting at rather low conductivity. The impedance study was conducted over a temperature range of RT–140 °C by repeating heating and cooling steps. The resulting Arrhenius plot is shown in Fig. 1b. A staggering six-order-of-magnitude difference was observed in the conductivity values of $LiZnSO_4F$-IL ($\sim 10^{-5}$ S cm^{-1}) and $LiZnSO_4F$-C ($\sim 10^{-11}$ S cm^{-1}) pellets. These values were reproducible in several measurements. Subsequently, we performed a DC polarization measurement in $LiZnSO_4F$ pellets in a special Swagelok architecture allowing only for Li^+ current as illustrated in Fig. 1c (inset). For different external voltages, we were unable to record any current in $LiZnSO_4F$-C sample affirming the rather insulating behavior. However, in case of $LiZnSO_4F$-IL sample, noticeable Li^+ current values were recorded signaling good Li-ion conductivity (Fig. 1c). Both the AC impedance spectrosco-

py and the DC polarization study were in perfect agreement showing a large difference in ionic conductivity of $LiZnSO_4F$-C and $LiZnSO_4F$-IL.

In our earlier work, we measured the conductivity values of Li-based fluorosulphates in the range of 10^{-11} S cm^{-1} [7]. Thus, the conductivity value of $LiZnSO_4F$-C is reasonable. However, the high conductivity value in the case of $LiZnSO_4F$-IL was a surprise, which can arise either due to structure or surface modification. $LiZnSO_4F$ stabilizes into a different structure (orthorhombic, s.g. *Pnma* [11]) than other $LiMSO_4F$ compounds (triclinic, s.g. *P*-1), which leads to a one-dimensional diffusion of Li for $LiZnSO_4F$ as compared to a three-dimensional one for $LiMSO_4F$ phases. It leads to the expectation of having a

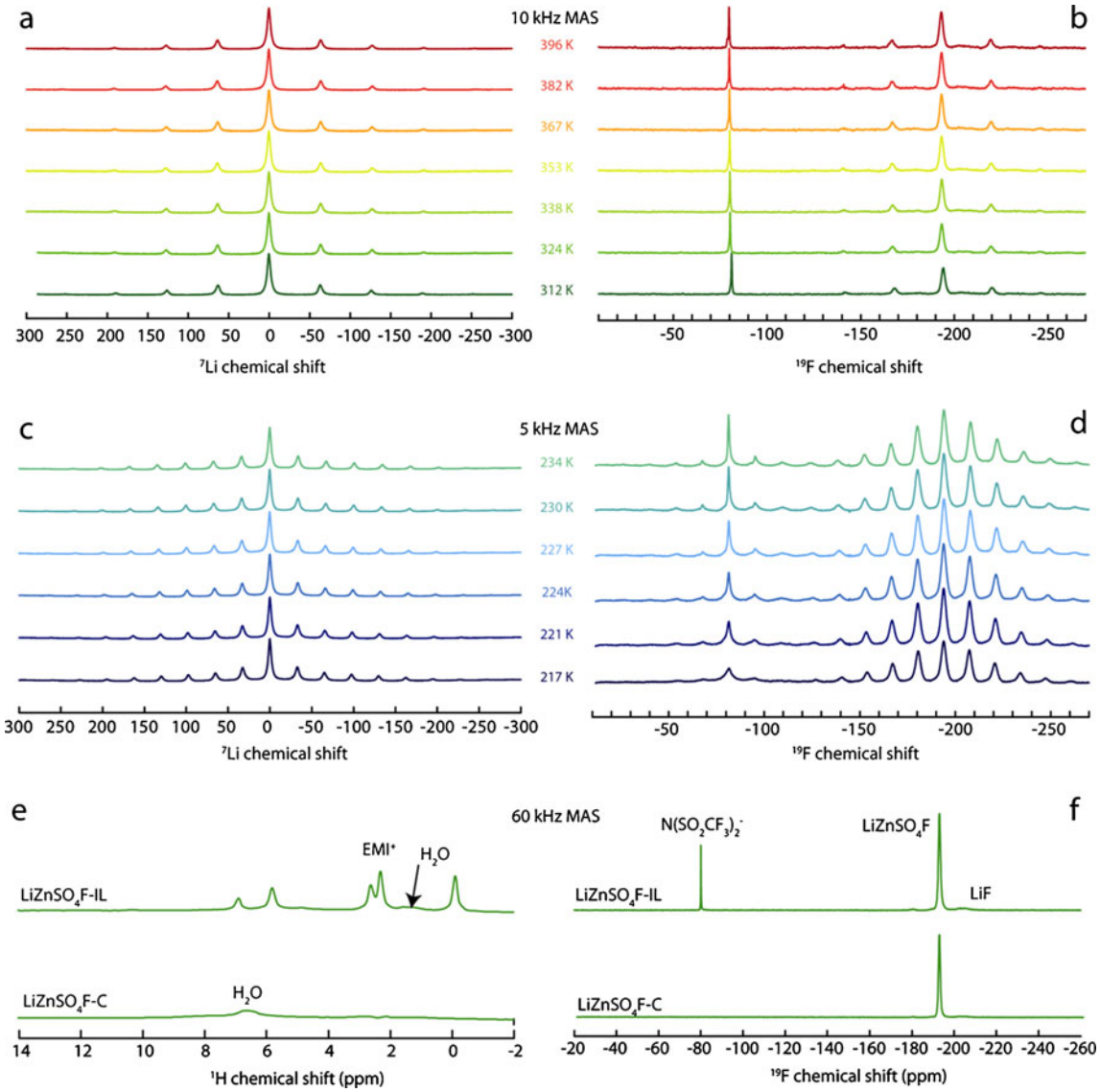

Fig. 2 Solid-state NMR ^{7}Li (**a**, **c**), ^{19}F (**b**, **d**, **f**) and ^{1}H (**e**) spectra. The spectra have been recorded between 312 and 396 K at 10 kHz MAS (**a**, **b**), while the spectra at low temperatures (**c**, **d**) between 217 and 234 K had to be recorded at 5 kHz MAS, both for $LiZnSO_4F$-IL. The ^{1}H and ^{19}F fast MAS (60 kHz) spectra (**e**, **f**) have been recorded without temperature regulation (≈320–340 K in the rotor) for both $LiZnSO_4F$-IL and $LiZnSO_4F$–C samples. No change in the ^{7}Li NMR spectrum is observed upon heating/cooling (**a**, **c**), seemingly indicating no change in the bulk $LiZnSO_4F$ lithium mobility. The mobile lithium atoms are not detected by NMR in these spectra. For ^{19}F NMR, no change is detected upon heating (**b**); however, the peak stemming from TFSI (−80 ppm) is considerably broadened below 220–230 K (**d**) indicating that the ionic liquid motions are frozen below these temperatures. A comparison between the high resolution ^{1}H (**e**) and ^{19}F (**f**) NMR spectra of $LiZnSO_4F$-IL and $LiZnSO_4F$–C clearly shows the presence of EMI and TFSI molecules in the samples (**e**, **f**), together with some residual water, either in $LiZnSO_4F$-C (≈6.5 ppm) or in the grafted ionic liquid layer for $LiZnSO_4F$-IL (≈1.8 ppm) (**e**). Some LiF is also detected by ^{19}F NMR (**b**, **f**)

lower ionic conductivity for the sillimanite $LiZnSO_4F$ than the tavorite $LiMSO_4F$ phases, the opposite of what we observed [7, 8, 11, 16]. So, solely from structural perspective, the high value of conductivity is difficult to explain. Thus, we turned our attention to probe possible surface modification in case of $LiZnSO_4F$-IL material.

First, we employed solid-state NMR spectroscopy on $LiZnSO_4F$-IL powder, which was feasible owing to the nonparamagnetic Zn center. ^{7}Li and ^{19}F spectra were obtained independently at different temperatures using a cryogenic set up. The ^{7}Li spectrum showed only one kind of Li species in the $LiZnSO_4F$ lattice (Fig. 2a). No change was detected for lithium when the temperature was varied between 217 and 396 K (Fig. 2a and c). In the ^{19}F spectrum, the ^{19}F signal from the bulk $LiZnSO_4F$-IL (−193 ppm) shows spinning sidebands induced by Magic Angle Spinning (MAS) when the MAS rate is lower than the chemical shift anisotropy (CSA). In addition to this signal, a weak LiF signal is observed around −204 ppm. Interestingly, a narrow signal appears at −80 ppm in $LiZnSO_4F$-IL (Fig. 2b, d, and f). This mobile species was assigned to the CF_3 group that arises from the TFSI anion of ionic liquid used in this work to prepare $ZnSO_4{\cdot}H_2O$-IL precursor. In the case of $LiZnSO_4F$-C sample, this extra peak (~80 ppm) was absent with only the peak arising from the F lattice atoms (Fig. 2f). The peak from TFSI shows strong broadening when the sample is cooled down to 220–230 K, indicating that the TFSI anion motion is considerably reduced below this temperature. Also, the ^{1}H NMR spectra of $LiZnSO_4F$ powders showed several extra H peaks in case of $LiZnSO_4F$-IL sample, which were solely assigned to the H-species present in the EMI-cation of the ionic liquid (Fig. 2e). Overall, the NMR investigation revealed the possible surface contamination of $LiZnSO_4F$-IL product by a slight amount of ionic liquid (EMI-TFSI).

We further pursued the surface analysis of $LiZnSO_4F$ sample by XPS analysis. Figure 3 shows C 1 s, F 1 s and N 1 s core peaks of $LiZnSO_4F$-IL and $LiZnSO_4F$-C samples. For $LiZnSO_4F$-IL, all spectra provide evidence for the presence of the ionic liquid at the surface of the sample. C 1 s peak at 292.8 eV and F 1 s peak at 688.6 eV are clearly assigned to CF_3 groups of TFSI-anion. The three kinds of environments of carbon in the EMI-cation (C–C, C–N and N–C–N) are also detected in the C 1 s spectrum of $LiZnSO_4F$-IL. Moreover, EMI-cation and TFSI-anion show very characteristic N 1 s signatures in the N 1 s spectrum (399.4 eV and 401.8 eV, respectively). Taking into account that XPS measurement is carried out on the extreme surface of the samples (5 nm), quantitative analysis reveals that the amount of remaining ionic liquid at the surface of the $LiZnSO_4F$-IL sample is about 60 at.% (i.e., the ionic liquid layer is ~3 nm). Note that a third weak peak can be detected in the N 1 s spectrum of $LiZnSO_4F$-IL (400.6 eV) that could be attributed to some decomposition product of the ionic liquid.

With the NMR and XPS analysis, we confirmed the presence of some remnant ionic liquid at the surface of $LiZnSO_4F$-IL product. It was not obvious as the $ZnSO_4{\cdot}H_2O$-IL precursor was heat-treated mildly inside ionic liquid (at 150 °C for just 1 h) and was later washed several times with organic solvents (e.g., ethyl acetate) capable of dissolving ionic liquids. In spite of several washing steps and final heat treatment with LiF (at 300 °C for 30–40 h), the presence of ionic liquid in the $LiZnSO_4F$-IL product suggests strong binding of layers of ionic liquid on the surface of $LiZnSO_4F$ particles. From the NMR signal, we could roughly quantify the amount of ionic liquid present. A quick back-of-envelope calculation estimated an 8–15-nm monolayer of ionic liquid (EMI-TFSI) covering the micrometric grains of $LiZnSO_4F$, which is

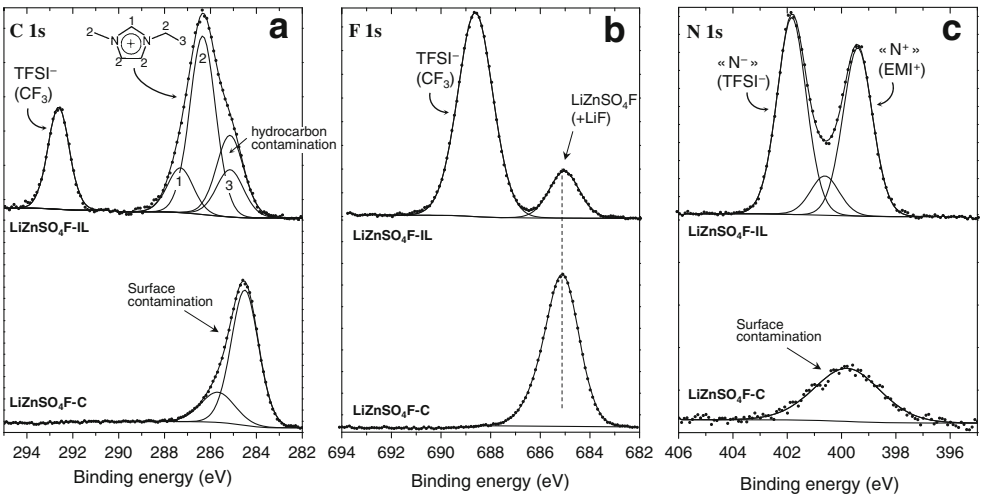

Fig. 3 XPS spectra probing the **a** C 1 s, **b** F 1 s and **c** N 1 s peaks in the case of $LiZnSO_4F$-C and $LiZnSO_4F$-IL powder samples. Some extra peaks arise in $LiZnSO_4F$-IL sample, which can be assigned to TFSI-anion and EMI-cation. This confirms the presence of the ionic liquid (EMI-TFSI) in the final $LiZnSO_4F$-IL product

overestimated from what we deduced by XPS. Inhomogeneity in the surface coverage could be at the origin of such a difference. Here, we would like to mention that we failed in our attempts to capture direct evidence of ionic liquid graft on $LiZnSO_4F$ particles by (SEM/TEM) microscopy as the ionic liquid containing fluorosulphate samples were unstable and were prone to decomposition under high voltage electron beam.

This led us to the model of 'ionic liquid grafting' as illustrated in Fig. 4. During the heat treatment of $ZnSO_4{\cdot}7H_2O$ precursor submerged in the EMI-TFSI ionic liquid bath, the hydrophobicity of ionic liquid pacify the kinetic of removal of extra structural water. During this process, some ionic liquid is attached to the surface of $ZnSO_4{\cdot}H_2O$ monohydrate precursor. Being a surface phenomenon, this ionic liquid grafting essentially depends on wettability, catalytic/chemical reactivity as well as surface truncation of precursor solid and the type of ionic liquid. This ionic liquid graft is permeable to H_2O, Li^+ and F^- species, so it facilitates the double ion exchange reaction (i.e., H^+ by Li^+ and OH^- by F^-) at 300 °C forming $LiZnSO_4F$ product. As it is a topotactic reaction involving minimal volume change [7, 8], the grafted ionic liquid layer remains intact in the final product. As ionic liquids are capable of solvating Li^+, it is possible for the ionic liquid layer to trap some Li^+-ion either from excess LiF precursor or from the outer surface of $LiZnSO_4F$. So, a final model can be visualized as slight Li-deficient $LiZnSO_4F$ particles wrapped up by a Li-rich ionic liquid graft, providing a percolation network for easy Li-ion mobility.

Next, we tried to generalize the concept of IL-grafting induced conductivity enhancement in other members of the Li-metal fluorosulphate family. In order to show that the IL-grafting effect is independent of crystal structure, we chose anisostructural tavorite $LiCoSO_4F$ (triclinic, $P\text{-}1$) and triplite $LiMnSO_4F$ (monoclinic, $P2_1/c$). These phases were prepared using $MSO_4{\cdot}H_2O$ (M = Co, Mn) made both by ionic liquid and ceramic route. The structural and transport properties of these materials are summarized in Fig. 5. The structural details of $LiCoSO_4F$ and $LiMnSO_4F$ phases are given elsewhere [8, 16]. In each case, we obtained nearly uniform micrometric particles (~1 μm). Interestingly, we noticed six-order-of-magnitude difference in ionic conductivity values of $LiMSO_4F$-C (~10^{-11} S cm^{-1}) and $LiMSO_4F$-IL (~10^{-5} S cm^{-1}) samples in each case. While $LiMSO_4F$-IL samples had low activation energy (~0.25–0.3 eV), the $LiMSO_4F$-C samples had high activation energy (~0.6–0.75 eV). It reassures forming a Li-ion conducting ionic liquid graft at their inter-granular interface can enable the ionic conductivity of insulating fluorosulphate ceramics. Nevertheless, we would like to stress that we did not detect the same effect for tavorite $LiFeSO_4F$, in which case the ionic conductivity value remained same (~10^{-11} S cm^{-1}) independent of the

Fig. 5 Generalization of the concept of 'ionic liquid grafting' as a way to improve Li-ion conductivity in various anisostructural alkali metal fluorosulphates. Similar phenomena were marked in **a** sillimanite $LiZnSO_4F$ (*left column*), **b** tavorite $LiCoSO_4F$ (*center column*) and **c** triplite $LiMnSO_4F$ (*right column*). In each case, the XRD pattern, crystal structure, representative SEM image (showing micrometric particles) and Arrhenius plots showing ac conductivity is given. The presence of ionic liquid grafting at the particle interface triggers six-fold improvement in ac conductivity in each case

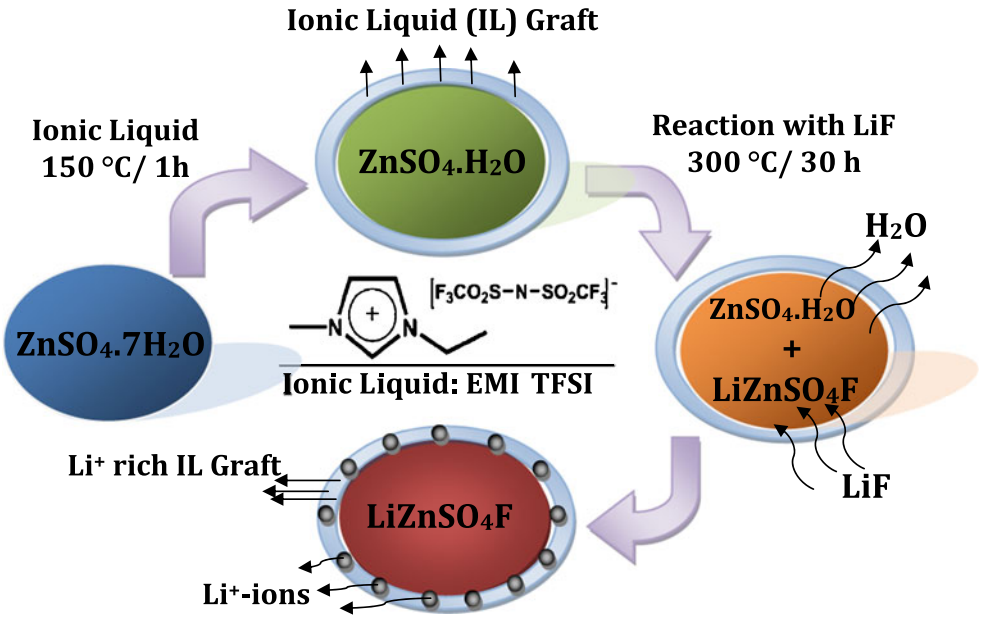

Fig. 4 *Schematic flow diagram* depicting the formation of monolayer of ionic liquid grafting at the interface of $ZnSO_4{\cdot}H_2O$ monohydrate precursor during dehydration. This ionic liquid graft is permeable to Li, F, H and OH species so as to allow the simultaneous departure of H_2O and the ingression of LiF. The 'ionic liquid grafting' thus remains intact in final $LiZnSO_4F$ product, which is slightly Li-rich and forms an easy percolation network for Li^+ ion movement

$LiZnSO_4F$ *Sillimanite* (*Pnma*)	$LiCoSO_4F$ *Tavorite* (*P*-1)	$LiMnSO_4F$ *Triplite* ($P2_1/c$)

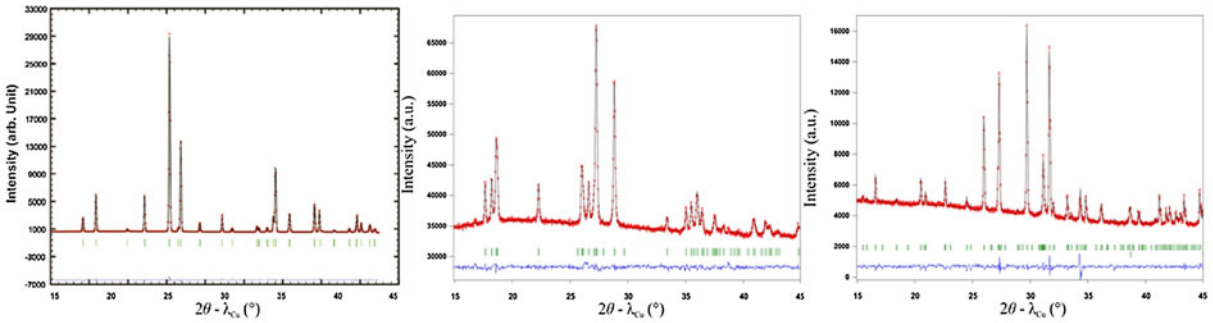

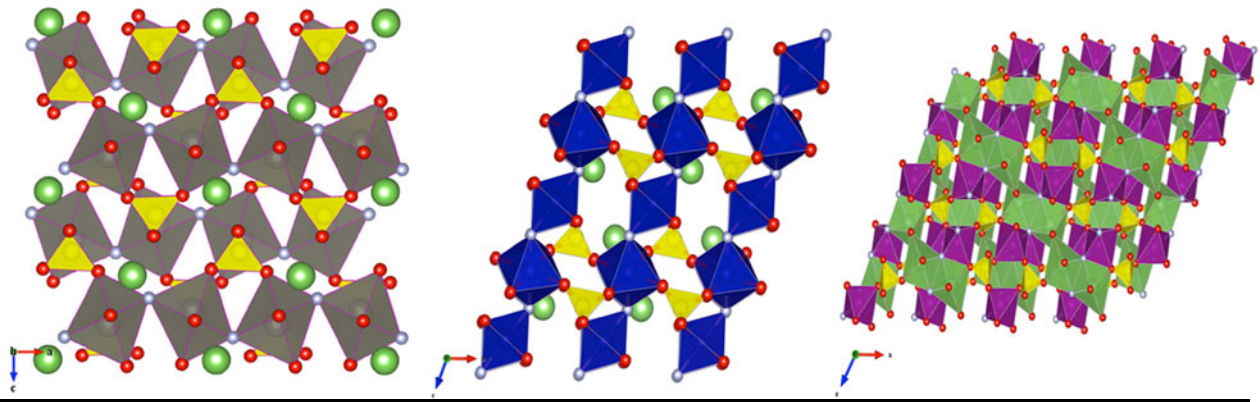

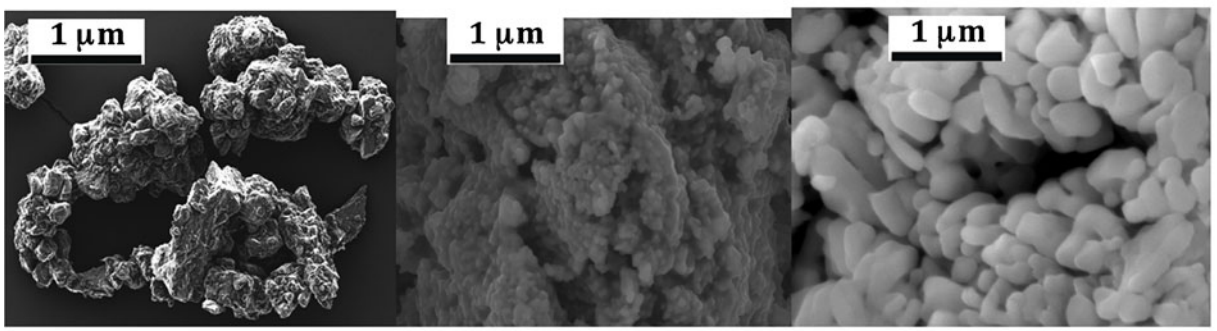

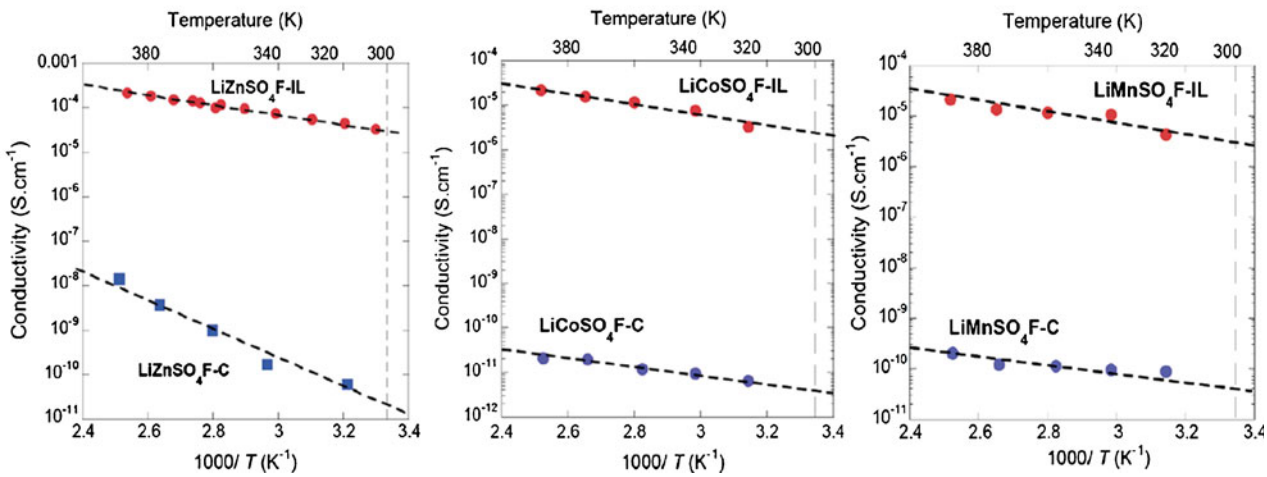

processing routes ($LiFeSO_4F$-IL and $LiFeSO_4F$-C). Though we do not have complete understanding of these results, presumably the ineffective formation of interfacial ionic liquid grafting is at the root of such behavior. The feasibility and factors controlling the effective formation of ionic liquid grafting can shed light on these intricate issues.

This kind of conductivity improvement owing to modified interface does not come as a surprise as several such routes have been reported in the field of 'solid-state ionics' as illustrated in Fig. 6. For example, olivine $LiFePO_4$, one the most sought after cathode material offering very high capacity at safe operating voltage of 3.45 V suffers from low ionic conductivity (~10^{-12} S cm^{-1}), thus, limiting its rate capability. A recent report proves the transport properties of $LiFePO_4$ can be improved by forming a thin (~5 nm) interface layer of Fe^{3+}-containing amorphous $Li_4P_2O_7$-like phase around each grain [17]. As a result, ultrafast charging and discharging rate was realized in $LiFePO_4$ cathode with excellent cycling stability at room temperature. Another such example is the manifold improvement in the conductivity of fluoride materials (BaF_2/CaF_2) by formation of interfacial 'space charge'. The degree of this space charge layer can enhance the room temperature conductivity by three orders of magnitude [18]. Yet another interfacial modification method, namely 'ionic liquid tethering', was recently reported showing the attachment of ionic liquid molecules in ceramic oxides (TiO_2 or ZrO_2) can improve its mechanical strength as well as conductivity by two orders of magnitude [19]. Drawing parallel to these methods, we propose 'ionic liquid grafting' as an attractive way of

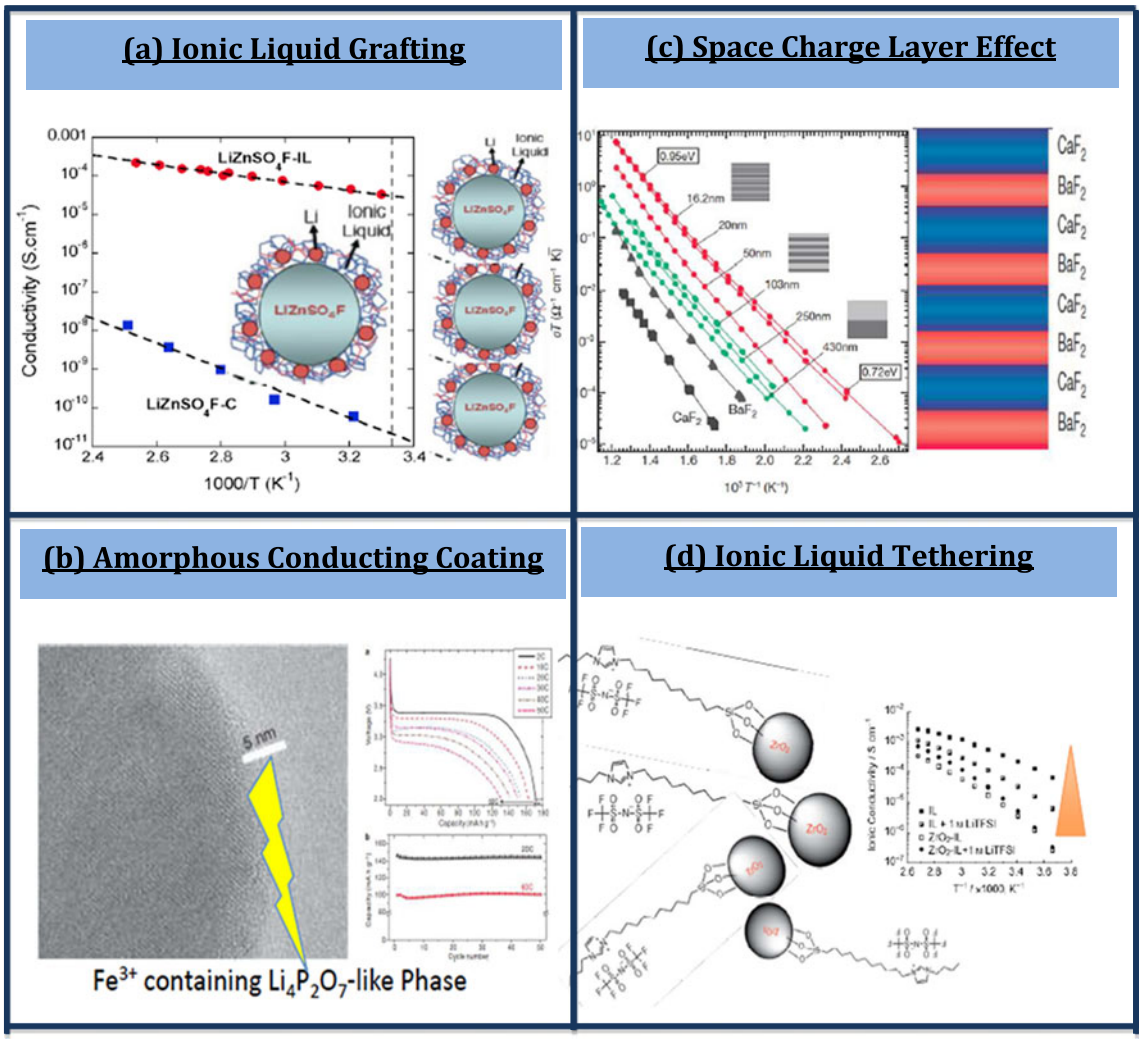

Fig. 6 The transport properties of ceramic materials can be improved by forming a thin interfacial layer of conducting species. One such method is **a** ionic liquid grafting, which is conceptually analogous to several previously reported methods like **b** amorphous conducting coating of $LiFePO_4$ [17], **c** formation of space charge layer [17], and **d** ionic liquid tethering [18]

interface engineering to enable the transport properties of inherently insulating materials.

Conclusions

With the principal goal to design a novel Li-based fluorosulphate as a solid-electrolyte material, we synthesized the sillimanite-structured $LiZnSO_4F$ compound. Though it had very low conductivity (~10^{-11} S cm^{-1}), we accidentally discovered the possibility of manifold improvement in conductivity of $LiZnSO_4F$ ceramic by forming a monolayer of ionic liquid at its interface. Using several spectroscopy techniques, we proved the existence of ionic liquid grafted at the particle surface and its positive effect in improving the ionic conductivity. This phenomenon was successfully extended to other anisostructural fluorosulphate members. Future research may focus on further understanding and controlling of ionic liquid graft formation at grain interface, which can extend this method to conventional oxide and polyanionic solid electrolytes. 'Ionic liquid grafting' can be an alternate method to develop ceramic–ionic liquid composites with high ionic conductivity approaching those needed for solid-electrolyte applications.

Acknowledgements The scientific assistance of Dominique Massiot (Orleans) and Danielle Gonbeau (Pau) is acknowledged. We thank ALISTORE-ERI for the financial support. The first author (PB) is grateful to the Japan Society for the Promotion of Science for a JSPS Fellowship at the University of Tokyo.

References

1. Mizushima K, Jones PC, Wiseman PC, Goodenough JB (1980) Mater Res Bull 15:783–789
2. Padhi AK, Nanjundaswamy KS, Goodenough JB (1997) J Electrochem Soc 144:1188–1194
3. Nyten A, Abouimrane A, Armand M, Gustafsson T, Thomas JO (2005) Electrochem Commun 7:156–160
4. Yamada A, Iwane N, Harada Y, Nishimura S, Koyama Y, Tanaka I (2010) Adv Mater 22:3583–3587
5. Ramesh TN, Lee KT, Ellis BL, Nazar LF (2010) Electrochem Solid-State Lett 13:A43–A47
6. Nishimura S, Nakamura M, Natsui R, Yamada A (2010) J Am Chem Soc 132:13596–13597
7. Recham N, Chotard JN, Dupont L, Delacourt C, Walker W, Armand M, Tarascon JM (2010) Nat Mater 9:68–74
8. Barpanda P, Recham N, Chotard JN, Djellab K, Armand M, Tarascon JM (2010) J Mater Chem 20:1659–1668
9. Barpanda P, Chotard JN, Recham N, Delacourt C, Ati M, Dupont L, Armand M, Tarascon JM (2010) Inorg Chem 49:7401–7413
10. Sorokin NI, Sobolev BP (2007) Crystallogr Rep 52:842–863
11. Barpanda P, Chotard JN, Delacourt C, Reynaud M, Filinchuk Y, Armand M, Deschamps M, Tarascon JM (2011) Angew Chem Int Ed 50:2526–2531
12. Armand M, Gauthier M, Magnan JF, Ravet N (2004) US Patent 033:360
13. Rodriguez-Carvajal J (2001) CPD Newslett 26:12–19
14. Momma K, Izumi F (2008) J Appl Crystallogr 41:653–658
15. Bielecki A, Burum DP (1995) J Magn Reson A 116:215–220
16. Barpanda P, Ati M, Melot B, Rousse G, Chotard JN, Doublet ML, Sougrati MT, Corr S, Jumas JC, Tarascon JM (2011) Nat Mater 10:772–779
17. Kang B, Ceder G (2009) Nature 458:190–193
18. Sata N, Eberman K, Ebert K, Maier J (2000) Nature 408:946–949
19. Schaefer JL, Moganty SS, Archer LA (2011) J Mater Chem 21:10094–10101